Exp # 595
FERMILAB-CONF-79-111-E

UR 730 (Oct 1979)
COO-3065-253

SOURCES OF PROMPT LEPTONS IN HADRONIC COLLISIONS*

Arie Bodek**
Department of Physics and Astronomy
University of Rochester, Rochester, N. Y. 14627

Published in AIP Proceedings No. 59, p. 211.

Invited Talk at the Annual Meeting of the Division of Particles and Fields of the Americal Physical Society, McGill University, Montreal, Canada Oct.79

Table of Contents

I. Introduction and historical perspective 1
II. The total prompt muon rate 3
1. Experimental Apparatus (Caltech-Fermilab-Rochester-Stanford)
2. Analysis
3. Discussion
4. Single muons and charm production
III. Investigation of the charm production contribution 6
1. Apparatus (Caltech-Stanford)
2. Analysis
3. Single muon results
4. Two prompt muons with missing energy
5. Interpretation
6. Discussion
7. Comparison with beam dump experiments
IV. Search for bottom states 10
1. Bottom production analysis
2. Conclusion
3. Discussion
V. Conclusions 14

Appendix I. Sources of non-prompt leptons 15
1. Non-linearities (muons)
2. Fake Intercept (muons)
3. Non-direct electrons and non-promt electron neutrino sources
Appendix II. Sources of Prompt Dileptons 16
Record of Questions 18
References 19
Figures 23
Tables 28

*Work supported in part by the U.S.Department of Energy under Contract No. EY-76-C-02-3065.
**Alfred P. Sloan Foundation Fellow.

FERMILAB-CONF-79-111-E

SOURCES OF PROMPT LEPTONS IN HADRONIC COLLISIONS*

Arie Bodek**
Department of Physics and Astronomy
University of Rochester, Rochester, N. Y. 14627

ABSTRACT

Experimental evidence for various sources of prompt leptons produced in hadronic collisions is discussed. Emphasis is placed on sources of prompt single leptons and prompt multileptons. Such final states are expected from production and subsequent weak decays of short lived states. Hadronic charm production cross sections of 20 μb per nucleon at 400 GeV account for the observed single lepton signal as well as dileptons with missing energy (indicative of final state neutrinos). Limits of 40 μb/nucleon for bottom particle production in 400 GeV proton collisions are extracted from multimuon final state signatures. Various prompt dilepton sources (such as Drell-Yan and resonance production) are also summarized.

I. INTRODUCTION AND HISTORICAL PERSPECTIVE

The subject of prompt muon production in hadronic collisions has been investigated for a sufficiently long time to have been reviewed by two[1,2] Physics Reports articles. The first review article by Lederman[1] was published in 1976, and the second article by Craigie[2] was published in 1978. Therefore, I will not elaborate much on the historical development of the field or on the early data.

Investigations of prompt lepton production sources have resulted in several important discoveries and measurements. I will only mention a few highlights. The J/ψ was simultaneously discovered in e^+e^- collisions at SLAC[3] and in a hadronic dilepton experiment at BNL[4]. The Υ was discovered in a hadronic dilepton experiment at Fermilab[5], and high energy dimuon data has been used to extract nucleon[6] and pion[7,8], structure functions. Recently, new results on prompt single muon production[9,10], prompt neutrino production[11] and prompt dileptons with missing energy[12] have determined for the first time the level of charm production in hadronic collisions. In addition, limits on bottom particle production have been extracted[13] from data on prompt multimuon final states, and that technique looks promising as a tool for experiments to measure bottom particle production cross sections[14]. Multimuon final states can also be used to enhance bottom state signals in multiparticle spectrometer data[15] or in emulsions[16]

In this review I will discuss dilepton sources only briefly in Appendix II. Dileptons are reviewed in detail by A.J.S. Smith[17] at

*Work supported in part by the U.S.Department of Energy under Contract No. EY-76-C-02-3065.
**Alfred P. Sloan Foundation Fellow.

this conference. I will concentrate instead on prompt leptons that come predominantly from the production and subsequent weak decay of short lived states (i.e. charm and bottom states).

Historically[1,2] early data on prompt lepton production has been obtained by small acceptance single arm experiments. This prompt lepton data has been presented and lepton/pion yields. The advantages of that approach were:

1. Data from various energies (s), X_F, P_T and several nuclear targets could be plotted on the same linear scale (lepton/pion $\approx 10^{-4}$).
2. Some experimental uncertainties in acceptance would cancel if both lepton and pion data were measured in the same apparatus.
3. In prompt muon experiment, the π yield can also be extracted from the π decay muons, and thus the apparatus acceptance would also cancel in the ratio.

The disadvantages of the lepton/pion measurements were that they told us little about the sources of prompt leptons. The experiments were valuable in establishing the existence of a prompt muon signal in various s, X_F, P_T regions, and provided the motivation for the design of second generation experiments to study the phenomenon in detail. These experiments were designed to investigate particular final states. For example, the study as to whether prompt leptons come from single or pair sources required a large acceptance detector to identify second muons as well as a high density detector to minimize pion and kaon decays[9,10]. Such a detector is also suitable for multimuon studies[12,13]. On the other hand, detailed studies of dilepton final states require high resolution. Such resolutions were obtained in two arm spectrometers[4,5,6] and in open geometry large acceptance spectrometers[7,8].

Prompt muons are defined to be muons originating directly at the primary vertex or originating from the decays (e.g. weak or electromagnetic) of short lived states. Short lived is somewhat experiment dependent but is typically defined as particles with lifetime $(C\tau) \lesssim 1$ cm. Using this criteria we find that all strange particles are relatively long lived (see Appendix I).

Direct electrons is a term used to designate electrons that are not only prompt (i.e. from short lived states) but also do not originate from Dalitz decays such as $\pi_o \rightarrow \gamma e^+e^-$ and $\eta \rightarrow \gamma e^+e^-$. Dalitz decay contributions are usually not subtracted from prompt muon signals because the π^o does not decay to muons and the muonic Dalitz decays of the η and other particles are very small (see Table III).

The major sources of background in direct electron experiments are photon conversions, Dalitz decays and Ke3 decays. The major sources of backgrounds for prompt muon experiments are pion and kaon two body decays. The sources of non-prompt leptons for both types of experiments are discussed in Appendix I.

The contribution of pion and kaon decay muons is determined by measurements of the muon rate as a function of target and absorber density (ρ). The decay probability of pions and kaons is linearly proportional to the mean free path before interaction. This path is proportional to $1/\rho$. Therefore, the intercept of the prompt muon rate plotted versus $1/\rho$ at $1/\rho=0$ is the prompt muon signal. If the

target and absorber are a single unit, then the π decay muon rate would extrapolate to zero because the density is changed for pions from primary and secondary collisions at the same time[9,10].

Early prompt muon experiments[18,19] have used a different method. They used a fixed target and a movable absorber. The fake prompt signal due to interactions in the absorber had to be subtracted using Monte Carlo calculations[18].

The expected weak decay sources of prompt leptons are shown in Table I. These are mostly single lepton sources. Wherever experimental values for the lifetimes and branching ratios are not available, I have inserted a theoretical estimate designated with a (TH). Table II lists the particles that yield dileptons from electromagnetic sources, and have equal branching ratios to electron and muon pairs. Table III lists short lived sources which have different branching ratios to electrons and muons (mostly Dalitz decays). Here, wherever the branching ratio was not measured, I have included a rough estimate (RE) by using the measured photon decay mode as an input. Table IV lists sources of prompt multileptons that come from double weak decays and bottom particle cascade decays. Here a lot of the branching ratios are theoretical estimates. The non-prompt background sources are listed in Appendix I.

II. THE TOTAL PROMPT MUON RATE

Recently, the total prompt muon production rate for almost the entire forward hemisphere has been measured[10]. The experiment (Fermilab experiment E595; Caltech-Fermilab-Rochester-Stanford) was done in the Fermilab N5 line using 350 GeV diffracted protons. There are some preliminary results from a short test run performed in Feb. 1979. Since these are first results from this experiment, I will discuss the apparatus and analysis in more detail.

II.1 Experimental Apparatus (Caltech-Fermilab-Rochester-Stanford)

The experiment was performed at low intensities, i.e. about 1×10^4 350 GeV protons per pulse. The incident protons interacted in a target-calorimeter consisting of 49 (76×76 cm^2) steel plates (a total of 2.44 m of steel). The plates were independently mounted on rails so that the interplate spacing (and thus the calorimeter density) can be varied. The calorimeter was followed by a muon range detector consisting of eighty-eight 3 m $\times$ 3 m $\times$ 5.08 cm steel plates interspersed with forty-two 3 m $\times$ 3 m $\times$ 3.2 cm liquid scintillation counters with wave-shifter light collectors[30], and twenty-two 3.2 $\times$ 3.2 m^2 spark chambers with magnetostrictive readout[31]. The amount of light for each muon in the scintillation counters (15 photoelectrons) was sufficient to allow discrimination between one and two muons by use of counter pulse heights alone. The range detector was followed by a 3.5 m magnetized steel toroidal muon spectrometer.

The trigger required a proton interaction in the calorimeter in coincidence with a muon that penetrated at least 5.75 m of steel. Because of the large size of the range detector, this trigger effectively selected all muons of momentum $P_\mu > 8$ GeV, corresponding to

almost the entire forward hemisphere in the center of mass (Fig. 2).

Most muons satisfying this trigger were due to the decay of pions and kaons. This non-prompt background was measured by uniformly expanding the first 38 plates (1.68 m of steel) of the calorimeter, thereby proportionally increasing the mean path length and decay probability of hadrons in this region. Data were taken at three different densities: fully compacted, expanded by a factor of 1.75, and expanded by a factor of 2.5. The mean density of the compacted calorimeter is about 3/4 that of steel since there are gaps between plates where scintillation counters are mounted.

II.2 Analysis

The muon event rate (i.e. events with at least one muon with $P_\mu > 8$ GeV) per interacting proton exhibits a linear dependence on inverse density, ρ (Fig. 3). The intercept at $1/\rho=0$ of $(3.95 \pm 0.40) \times 10^{-4}$ is the prompt rate. However, to get the total rate, events with two muons both satisfying the requirement $P_\mu > 8$ GeV must be counted twice. This rate, determined using the scintillation counters in the range detector after corrections for accidentals[32], is $(0.94 \pm 0.01) \times 10^{-4}$, giving a total prompt muon rate of $(4.89 \pm 0.40) \times 10^{-4}$ per interacting proton. This rate has been corrected for a density independent background ($8 \pm 4\%$) from decays occurring downstream of the expanded region. This contribution was determined by a measurement in which only the downstream portion of the calorimeter was expanded.

The above quoted rate is for a thick target and includes contributions from secondary and tertiary hadron and photon interactions. To extract the contribution of the first collision a shower development calculation was performed. The calculation was based on radial scaling parametrization of particle production data from hydrogen[33] modified for nuclear effects. The contribution from secondary and tertiary interactions was calculated[34] to be $(1.60 \pm 0.2) \times 10^{-4}$, and subtracted from the total prompt muon rate. The remaining rate of $(3.29 \pm 0.45) \times 10^{-4}$ is the prompt muon rate for primary collisions. We can express this rate as a $(\mu^+ + \mu^-)/(\pi^+ + \pi^-)$ ratio by dividing by the number of π's (with $P_\pi > 8$ GeV) produced by eacy primary proton collision. The number of π's of 3.55, extracted from the measured non-prompt muon rate and the shower development calculation[35], yields $\mu/\pi = (0.93 \pm 0.13) \times 10^{-4}$. The errors here are statistical. However, fairly conservative assumptions[36] yield an upper limit of 1.38×10^{-4} and a lower limit of 0.78×10^{-4}. The measurement is consistent with the trend of other μ/π data[37] at higher values of X_F as shown[38] in Fig. 4b. In a similar X_F and P_T region, ISR 30° data[39] (Fig. 4a) indicate that the average[40] e/π is between 3.2 and 4.8×10^{-4}. The data are in agreement with the trend established by another[41] ISR experiment at 90° although that experiment does not extend to low values of P_t (see Fig. 4a).

II.3 Discussion

There is about a factor of 4 difference between the 30° ISR e/π

results (Baum et al[39]) and the Fermilab μ/π data (Ritchie et al[10]). Although the two experiments are in a different energy range and looked at electrons and muons respectively, it is instructive to investigate possible reasons for the different results.

1. Ritchie et al. used a steel target, (p-Fe) while the ISR 30° data is for p-p. If all the difference were attributed to nuclear effects (p-Fe vs pp), then the A dependence of prompt muons at small X_F and small P_T would have to be $A^{0.43}$ (i.e. much less than the inelastic cross section which rises as $A^{0.70}$). Such an unusual A dependence is unlikely. For example, the A dependence of π production (for π's with $P_\pi > 8$ GeV) is $A^{0.79}$ yielding only a 30% difference between p-Fe (3.55 π's) and pp[33] (2.45 π's) interactions. Also, at higher $X_F (X_F \gtrsim 0.1)$ the A dependence for $\mu^+\mu^-$ pairs has been measured[42] to be $\sim A^{0.70}$ for low $M_{\mu\mu}$ and $A^{1.0}$ for high $M_{\mu\mu}$.
2. The center of mass energy at the ISR ($\sqrt{s}$=53 GeV) is larger than that of the Fermilab 350 GeV data ($\sqrt{s}$=23.7 GeV). This difference initially appeard unimportant since a low energy[43] experiment also indicated a large e/π ratio. However, the experimental situation at low energies is somewhat unclear since more recent low energy experiments[44] at SLAC and ANL indicate a <u>small</u> e/π ratio. We conclude that s-dependent effects cannot be ruled out.
3. Baum et al. measured e/π versus the μ/π measured by Ritchie et al.

It is possible that the source of low P_T electrons does not yield a corresponding rate of low P_T muons. This would be the case if the low P_T electrons were from low mass pairs (e.g. due to the muon-electron mass difference) rather than from, for example, charm decays. The ISR experimenters, based on their $e\mu$ measurements, have concluded[45] that charm production[46] is not the source of the large low P_T electron rate. Since that experiment vetoes on very low mass e-pairs, they conclude that the source of direct electrons at low P_T are e^+e^- pairs with m_{ee}>0.1 GeV. At the low P_T region there is a large contribution from Dalitz decays which must be calculated and subtracted. The Dalitz decay contribution (see Table III) may be larger than expected[48]. For example, the production cross section for η mesons at low P_T has not been measured, and high P_T measurements[49] (P_T>1 GeV) indicate a large η cross section ($n/\pi \simeq 0.5$). Therefore, a source such as copious η production at low P_T at ISR energies could account for the difference between the two experiments.

II.4 Single Muons and Charm Production

There are also some preliminary results regarding the contribution of prompt <u>single</u> muons to the total prompt muon rate. A preliminary separation of single muon and dimuon events (using the scintillation counters only) after corrections for misidentified dimuon events, yields a prompt single muon rate of $(1.05 \pm 0.5) \times 10^{-4}$, this rate indicates that at 350 GeV (30±15)% of the prompt muons

come from single muon sources. The prompt single muon rate can be used to obtain a charm production cross section. The acceptance for charm production is large (39±1%) and rather insensitive to model assumptions because muons from almost the entire forward hemisphere are detected. Using a semileptonic branching ratio of 8% and a linear A dependence one obtains a charm cross section of 22 ± 9 μb/nucleon.

The A dependence of prompt single muons originating from charm production is expected to be similar to the A dependence of ψ production (i.e. linear). On the other hand, the dimuon rate is dominated by low mass sources with an $A^{2/3}$ dependence. Therefore, the relative contribution of single vs. 2μ sources to the total prompt muon rate is expected to depend on the target material. High A targets (e.g. Fe) are expected to have a larger prompt single muon contribution than low A targets (e.g. H_2,Be). Similarly, the energy dependence of charm production is expected to be steeper than that for ρ meson and other low mass dimuon pairs. Therefore, prompt single muons are expected to contribute more to the promp muon rate at higher incident energies.

III. INVESTIGATION OF THE CHARM PRODUCTION CONTRIBUTION

In the previous section, it was mentioned that the contribution of prompt single muons to the total prompt muon rate is ≃30 ± 15%. Several years ago, it was pointed out by Bourguin and Gaillard[49] that the P_T dependence of muon from charm decays does not fall as steeply as the P_T dependence of muons from ρ and low mass dimuons. Similarly, because of the very steep P_T dependence of pions, it was expected that the background from π decay muons would be small for P_T values of around 1 GeV. I will now discuss the results of Fermilab experiment E379 (Caltech-Stanford)[9] which concentrated on the P_T region near 1 GeV.

III.1 Apparatus (Caltech-Stanford)

This experiment was the first to establish a prompt single muon signal[9] and reported on the observation of a prompt 1-μ signal in the moderately high P_T ($0.8<P_T^{\mu^+}<2.5$ GeV) and low X_F ($10<E^{\mu^+}<60$ GeV) region produced by 400 GeV p - N interactions. Approximately equal production cross-sections for 1-μ and 2-μ final states were found in this kinematic region. Evidence for the observation of missing energy (indicative of final state neutrinos) in association with hadronically produced $\mu^+\mu^-$ pairs, was presented and related to the observed single muon signal[12]. The calorimeter used in the missing energy investigation was the same one described in the previous section. The major experimental difficulties in the measurement of a prompt single muon signal come from:

1. Separating the π,K decay from the prompt signal.
2. Distinguishing 1μ from 2μ events.

The experimental approach taken was:

1. Vary the target-absorber density to determine the π,K decay background.

2. Maximize signal/background by triggering on a μ^+ in the high P_T region ($P_T \simeq 1$ GeV).
3. Greatest possible acceptance for identifying 2nd muons in di-muon events.
4. "Detection" of final state neutrinos by tagging missing energy in the final state.

The experimental apparatus is shown in Fig. 5.

The experiment was performed in the Fermilab N5 beam with 400 GeV protons at typical intensities of $3\text{-}5 \times 10^5$/sec. The primary elements of the detector (Fig. 5) were a fine-grained target-calorimeter of variable density (energy resolution of 3.5% at 400 GeV), a muon identifier (MI), and a toroidal muon spectrometer.

The data were taken with a high-P_T trigger, which required a coincidence of both a beam and a muon trigger component. The muon component required the muon to remain in the same quadrant throughout the toroid system by requiring the appropriate coincidence of counters C, S2, ACR, T4 (which were divided into quadrants) and S1, T2, T3, (divided into half-planes). This requirement preferentially selected muons with high P_T ($P_T^{\mu^+} > .8$ GeV).

The beam component required an incident proton to pass through counters B0 and B1 (7.6×7.6 cm and 5.1×5.1 cm) and to interact within the first 10 plates of the calorimeter. To reject any background from upstream interactions, triggers were vetoed by the presence of any additional particles in the beam or halo counters within 95 nanoseconds of the trigger. Further beam information was provided by the pulse height of the trigger counters and by the incident proton's trajectory and momentum, as measured by a spectrometer immediately upstream of the calorimeter. Interactions satisfying the beam trigger alone were scaled, and one out of each 2^{16} was recorded to provide a control sample of interactions without any muon requirement.

III.2 Analysis

The experiment collected data at three different densities (keeping the mean interaction point fixed in space): fully compacted, expanded by a factor of 1.5, and expanded by a factor of 2. The mean calorimeter density in the compacted configuration was 3/4 that of steel due to the gaps (1.3 cm) between plates. After all software cuts, the rates in each density configuration were normalized to the beam trigger rates and plotted as shown in Fig. 6. As expected, the 2-μ rate is flat, and the 1-μ rate shows a linear increase with the effective pion interaction length. The 1-μ slope measures the rate from non-prompt decays, and the intercept of $(10.5 \pm .5)10^{-6}$ at infinite density is the raw prompt 1-μ signal.

To obtain the true prompt single muon rate, the raw prompt 1-μ rate had to be corrected for several background sources:

a) $\mu^+\mu^-$ events with a low energy μ^- which ranged out in the calorimeter or muon identfier. A Monte-Carlo calculation using the measured $\mu^+\mu^-$ distributions gave a correction of 10±2% (systematic errors included) of the raw prompt 1-μ signal. This component was subtracted from the 1-μ signal and added to the 2-μ signal.

b) Muons from decays of pions and kaons in the unexpanded part of the calorimeter (after plate 25). A Monte-Carlo simulation of the hadron shower, which reproduced the mean shower profile measured in the experiment, gave a correction of 8±3% of the measured decay rate. This corresponds to 16±6% of the prompt 1-μ signal.

c) A subtraction of 20±10% of the prompt 1-μ signal due to second order variation in the acceptance with density. These arise because, although the mean interaction point stays fixed, multiple scattering effects and production by secondaries move downstream when the calorimeter is expanded. Since the toroid hole subtends a larger angle for particle originating downstream, this yields a reduction of 4±2% in the acceptance of the expanded relative to the compacted configuration. This correction was obtained from the $\mu^+\mu^-$ events (which should be constant with density).

III.3 Single Muon Results

After all corrections, the measured prompt 1-μ rate was $(5.8 \pm 1.5)\times10^{-6}$ per incident proton and the 2-μ rate was $(5.9\pm.2)\times10^{-6}$; the errors are largely systematic. These rates indicate that in the P_T region near 1 GeV prompt single muons account for 50±13% of all prompt muons.

III.4 Two Prompt Muons with Missing Energy

The total observed energy spectrum for $\mu^+\mu^-$ events ($E_{tot}=E_{\mu^+}+E_{\mu^-}+E_{calorimeter}$) is shown in Fig. 7. The dashed curve shown for comparison is the E_{tot} spectrum exhibited by beam interactions without final state muon. There is a pronounced enhancement of missing energy events for $m_{\mu^+\mu^-}<2.4$ GeV. We observe 227 $\mu^+\mu^-$ events with missing energy in excess of 45 GeV. An estimate of the double π,K decay background is provided by the 5 <u>observed like sign</u> dimuon events with large missing energy. Monte Carlo calculation of $K\bar{K}$ production and double decay also yields a background of 5 events. Also, since the toroid spectrometer is instrumented with acrylic calorimetry counters, we can rule our catastrophic muon energy loss in the steel as significant source of background. We conclude that all backgrounds are unlikely to contribute more than 10% of the observed $\mu^+\mu^-$ with missing energy signal.

III.5 Interpretation

To estimate a charm production cross-section from these data, we have assumed that all the signal comes from the semileptonic decays $D\to K\mu\nu$ (60%) and $D\to K^*\mu\nu$ (40%) with a total semileptonic branching ratio of 8%. The inclusive D cross-section was assumed to increase linearly with the atomic number A of the nucleus and was parameterized as

$$E\frac{d^3\sigma}{dp^3} = C\,(1-x_F)^{\beta}\,e^{-\alpha p_t} \text{ (for inclusive D production)} \qquad (1)$$

The single muon data were consistent with values in the range α=2.0-3.5 GeV^{-1} and β>3. Varying α and β over these allowed ranges yields charm cross-sections in the range 15-75 μb/nucleon. For β=3 and α=2.5, the acceptance for the produced μ^+'s was 2.8% and the cross-section for D production was $\sigma_{D\bar{D}}$=35±9 μb/nucleon. This model, in which the two charmed states are uncorrelated gives an acceptance of 0.22% for the $\mu^+\mu^-$ events with 45 GeV of missing energy and yields a charm cross-section of 17±3 μb. However, the $\mu^+\mu^-$ mass and momentum distributions do not fit this model. The 25% error in the charm cross section extracted from the single muon results and the 20% error in the cross section extracted from the 2μ results include experimental statistical and systematic errors (mostly systematic) but do not include model dependent undertainties in acceptance or branching ratios.

In order to include the expected correlation between the D and $\bar{D}$ state we assume a $D\bar{D}$ model production model

$$E\frac{d^3\sigma}{dp^3} = \frac{C}{M^3}\,(1-x_F)^{\beta}\,e^{-\alpha p_t}\,e^{-M/\sqrt{s}} \text{ (for } D\bar{D} \text{ production)} \qquad (2)$$

and calculated the fraction of $D\bar{D}$ double muonic decays which satisfy our trigger requirement, give 2 μ's that pass the muon cuts, and yield a measured missing energy in excess of 45 GeV. Here the kinematic variables in the above cross-section equation refer to the composite $D\bar{D}$ system (and $\sqrt{s}$=27.4). The acceptance was rather insensitive (to ±30%) to variations in α between 1.5 and 3.0 GeV^{-1} and γ between 0.0 and 17.5. For α=1.3, β=6 and γ=20 we obtain an acceptance of 0.27% yielding a charm cross section of 14±3 μb. Using this same model we obtain a charm cross-section of 21±5 μb from the single muon data. Changing β from 2.96 to 6.0 changes the $\mu^+\mu^-$ acceptance from 0.39% to 0.24%. (See Table 5.)

III.6 Discussion

In general the charm cross sections extracted from the 2μ data are lower than those extracted from the single muon data (see Table 5). Although for the best fit model parameter the extracted cross sections are consistent (14±3 and 21±5) closer agreement between the two sets of data is obtained with an average branching ratio of 5% which gives $\sigma_{charm}\simeq$35 μb/nucleon. In view of the recently reported difference between the D^o and D^+ semileptonic branching ratios, (see Table I). This may be indicative of large D^o/D^+ production ratio. It is theoretically expected that $\sigma_{D^o}\simeq 3\sigma_{D^+}$ (see Rosner, ref. 23). It is expected[23] that the fragmentation of charmed quarks would lead to final state charm particles in the following ratios: $1D^+$, $3D^o$, (0.7 to 2) F^+, and (0.9 to 2)Λ_c. Since the D^o,F and Λ_c have a smaller ratio than the charged D, average hadronic branching ratios

of order 5% are not unexpected.

The observation of a signal in both the single μ and 2μ plus missing energy signatures indicates that short lived hadronically produced states with branching ratio to muons of order 5% are produced with a total cross section of about 30 μb. Such a branching ratio indicates that the observed signal comes from charm rather than a new particle with a large muonic branching ratio such as $\tau^+\tau^-$ production ($\tau \to \mu\nu\nu$ BR is 17.5%). Theoretically it is expected that the cross section for $\tau^+\tau^-$ pairs is equal to the $\mu^+\mu^-$ Drell-Yan cross section for $\mu_{\mu\mu}$>4 GeV, i.e. a $\tau^+\tau^-$ production cross section of order 0.1 nb/nucleon. This cross section is much less than the observed 20 μb. Similarly, the observation of 2μ plus missing energy signal indicates that the muons do not originate from a copious production of a new particle which has a branching ratio to muons which is as small as those of the strange hyperons. The strange hyperon contribution is removed via the density extrapolation since the hyperons are relatively long lived. (See Appendix I.)

III.7 Comparison with Beam Dump Experiments

A detailed discussion of beam dump experiments can be found in the review talk by H. Wachsmuth[11] at the Batavia Lepton Photon (1979) Conference. Early beam dump results have indicated rather large cross sections (40 to 400 μb).[11] Recent runs yield smaller cross sections of order 15 μb which are in agreement with the prompt single muon results. The recent experiments have careful checks on upstream beam scraping and have data at different densities. The new data provided additional statistics to the small bubble chamber event sample. The 15 μb cross section assumes a linear A dependence and includes a correction for charm production by secondary interactions. The acceptance is model dependent. A production model for D mesons of the form

$$\frac{Ed^3\sigma}{d^3p} \sim (1-|x|)^n e^{-bp_t}$$

was used with n=3 and b=2. The cross sections are rather insensitive to b for b>2 but can vary[50] by a factor of 5 if n is changed from n=1 to n=5.

IV. SEARCH FOR BOTTOM STATES

Recently, there have been theoretical calculations, based on gluon vector-dominance models[51], which indicated large bottom particle production cross sections. Cross sections of the order of 200 nb for π^-N collisions at 150 GeV and 850 nb for p-p collisions at 400 GeV were predicted. Furthermore, experimental evidence has been reported[15] for the production of a heavy state (with a mass of 5.3 GeV) in π^-N collisions at 150 and 175 GeV. The size of the observed experimental cross section was large (≃200 nb). The decay mode[25] ($\psi K\pi$) of the state make it tempting to associate this state with the predicted B meson, i.e. a bound state of a b and $\bar{d}$ quark.

Bottom particle production is expected to lead to multimuon

final states (as shown in Table 4). Such final states were investigated using the same detector described in the previous section (Caltech-Stanford).

IV.1 Bottom Production Analysis

Three particular signatures of $B\bar{B}$ production and decay were investigated

1) $pN \to \psi\mu X$, i.e., a final state containing 3 muons, 2 of which reconstruct to a Ψ mass ($2.6\ \text{GeV} < M < 3.6\ \text{GeV}$) arising from $\bar{B}(B) \to \mu^+\nu X$, or $\bar{B}(B) \to \bar{D}(D)X$ with $D \to \mu\nu X$.
2) $pN \to \mu\mu\mu X$, a 3μ final state without any mass restriction arising from the following decay chain (or it charge conjugate):

   $B \to D\mu^-\nu$ with $D \to \mu^+ X$

   $\bar{B} \to \bar{D}\mu^+\nu$ with $\bar{D} \to$ hadrons

   or, alternatively,

   $B \to D\mu^-\nu$ with $D \to \mu^+\nu X$

   $\bar{B} \to \bar{D}X$ with $\bar{D} \to \mu^-\nu X$
3) $pN \to \mu^+\mu^+X$, arising from

   $B \to DX$ with $D \to \mu\overset{+}{\nu} X$

   $\bar{B} \to \bar{D}\mu^+\nu$ with $\bar{D} \to$ hadrons

The experimental features which make the experimental setup particularly suited for bottom particle investigations are:

1. The trigger required one high p_t muon ($p_t \gtrsim 0.8$ GeV) which enhanced muons from ψ and B particle decays.
2. The high density of the apparatus ($= \frac{4}{3}\rho_{Fe}$) minimized muons from π and K decay.
3. Background multimuon events arising from an extra muon unassociated with the interaction were eliminated by running the experiment at moderately low intensities (5×10^5 protons/sec) and vetoing triggers if there were any additional beam particles in beam or halo counters within ±95 nsec of the trigger. All muons were required to be in time with the interaction and to extrapolate to a vertex inside the calorimeter.
4. The probability for other background muons (primarily from π and K decay in the hadron shower) was directly measured by triggering the apparatus on random proton interactions without any muon requirement. In addition, the contribution of π- and K-decays to multimuon events was checked by comparing multimuon rates at different calorimeter densities.
5. Signal/background could be enhanced by the requirement of missing energy associated with bottom particle decays or the requirement of a high p_t muon associated with such decays.

The efficiencies for the detection of specific final states were calculated using the following assumptions about $B\bar{B}$ production and decay modes:

a) B's are produced via the reaction

$$p + Fe \rightarrow B + \bar{B} + \ldots$$

with the invariant cross section given by

$$E \frac{d^3\sigma}{dp^3} = \frac{1}{M^3} (1-x)^{\alpha} e^{-\beta p_t} e^{-\gamma M/\sqrt{s}}$$

where x_F, p_t and M refer to the compound $B\bar{B}$ system (with $M \gtrsim 10.6$ GeV), and $\alpha = 3.0$, $\beta = 2.2$, and $\gamma = 15$.

b) The cross-section follows linear A dependence.

c) The leptonic decay mode of the B proceeds via

$$B \rightarrow D\mu\nu$$

d) The nonleptonic decay mode of the B proceeds via

$$B \rightarrow D\pi\pi$$

e) All the ψ final states resulting from the B decay are represented by

$$B \rightarrow \psi K\pi$$

The detection efficiencies are only mildly dependent on these production and decay assumptions. However, the determination of $B\bar{B}$ production cross-sections from multimuon signatures is obviously dependent on the branching ratio assumptions. The assumptions used were $B \rightarrow \psi X = 3\%$, $B \rightarrow D\mu\nu = 10\%$, $B \rightarrow DX = 100\%$, and $D \rightarrow \mu\nu K$ (or K^*) = 8% (with a K/K^* ratio of 1.5). It was assumed, for simplicity, that the charged and neutral states have equal semileptonic branching ratios.

The trigger efficiencies, as well as the final acceptance after all analysis cuts on the muons, were calculated for each final-state category using a Monte Carlo simulation of the apparatus. These efficiencies, with the assumed branching ratio into each final state, are summarized in Table 6. Included, as subcategories, are the effects of additional cuts in p_t and missing energy which serve to enhance signal/background. The sensitivity (i.e., partial cross-section per detected event), given in the fourth column, is the product $\sigma_{pN}/(N_p\varepsilon)$, where σ_{pN}=13 nb/nucleon is the p-N cross-section on iron nuclei, $N_p = 1.01 \times 10^{10}$ is the total number of interacting protons (after dead time correction and cuts), and ε is the acceptance for detecting the final state muons. The inclusive $B\bar{B}$ cross-section per event in the last column is obtained from the partial cross-section/event using the branching ratio in column 5.

Table 7 summarizes the number of detected events in each category, the estimated background, and the resulting signals. Only data from the compacted density are used here, since backgrounds are smaller. Backgrounds arise from a single uncorrelated muon accompanying a ψ, $\mu^+\mu^-$, or μ^+ final state, and were calculated from the production rate of single muons which satisfied all analysis requirements. A μ^+ rate of $(2.5 \pm .6) \times 10^{-4}$/interaction and a μ^- rate of $(5.5 \pm 1.1) \times 10^{-4}$/interaction were measured in this experiment using the sample of random proton interactions taken throughout the run.

The difference between μ^+ and μ^- rates was due to acceptance; low energy μ^+'s were focussed into the toroid hole and then failed the analysis cuts. The backgrounds in coincidence with a ψ or $\mu^+\mu^-$ were estimated to be ≈15% smaller because of the reduction in hadron shower energy due to the production of the dimuon pair. In the case of $\psi\mu$ final states, for example, the background of 3.0 events is the product of 4399 recorded ψ's times an estimated rate of 6.8×10^{-4}/ interaction for an accompanying uncorrelated μ^+ or μ^-.

As a check of these background estimates, multimuon events taken at three different densities are compared in Fig. 8. The curves give the shape expected if the extra muons were entirely due to π and K decay backgrounds. It is evident that most, if not all, of the events are due to this background.

IV.2 Conclusion

None of the categories recorded in Table 8 shows any evidence of a positive signal (with the possible exception of the single event which survives the p_t cut in category 1a). We conclude from the limits in column 5 that $\sigma_{B\bar{B}} \leq 40$ nb. This is much smaller than the 850 nb predicted by gluon vector dominance model[51] and is also smaller than the 200 nb indicated[15] in 150 GeV π^-N interaction. The limit is in agreement with QCD calculations[55] indicating a $B\bar{B}$ cross section of 10 nb in 400 GeV pp collisions.

IV.3 Discussion

The disagreement with the predictions of the gluon vector dominance model[51] is probably not surprising in view of the fact that the same model[51] predicts a charm cross section of 170 μb in 400 GeV proton collisions. This charm cross section is also larger than the 20 μb indicated by the single muon results reported here. It may be possible to change the gluon distribution such as to reduce both the charm and bottom particle production cross sections, and bring the theory closer to agreement with the data. However, in any model dominated by gluon interactions high energy protons (e.g. 400 GeV) would be <u>more effective</u> in producing bottom states than low energy pions (e.g. 150 GeV). On the other hand protons would be <u>less effective</u> than pions if quark-antiquark annihilation processes were important. Such is the case in Υ production processes where pions are more effective than protons. Figure 9 shows Υ production cross section from J. Badier et al.[52]. Using the measured[52] value for $\sigma_\Upsilon \times (BR \to \mu^+\mu^-)$ of (1.5 ± 0.5)pb/nucleon in 200 GeV π^-N collisions and extrapolating to 150 GeV we obtain $\sigma_\Upsilon\ (BR \to \mu^+\mu^-) \simeq (1 \pm 0.5)$. The corresponding cross section for 400 GeV protons[53] is $0.5 \pm .24$ pb/nucleon. Therefore, if bottom particle cross sections were proportional to the Υ cross section, then 150 GeV π^- would be about twice as effective as 400 GeV protons in producing botton states (note the large errors, the ratio is 2 ± 1.4).

One can make the observation that the relation between ρ and π production is

$$\frac{\sigma_\pi}{\sigma_\rho} \simeq 10$$

and for strange particles

$$\frac{\sigma_K}{\sigma_\phi} \simeq 15$$

and for charm (400 GeV protons)

$$\frac{\sigma_{charm}}{\sigma_\psi} \simeq 100$$

where we have used a charm cross section of 20 μb and a ψ cross section[54] (measured in the same experiment) of $\sigma_\psi \cdot BR(\psi \to \mu\mu) = 17$ nb with $BR(\psi \to \mu\mu) = 0.07$. If $\sigma_{B\bar{B}}/\sigma_\Upsilon \approx 100$ we obtain (using [27] $BR(\Upsilon \to \mu\mu) = 2.3 \pm 1.4\%$ from Table II). $\sigma_{B\bar{B}} \approx 2$nb/nucleon which is consistent with the 40 nb limit.

In the case of ψμ final states a more direct comparison with the data of Barate et al. can be made. One would expect $\sigma(B\bar{B} \to \psi K\pi) \simeq 3\sigma(B\bar{B} \to \psi\mu)$ since $BR(B \to \psi K\pi)/BR(B \to \psi X) \simeq 0.5$ and $[BR(B \to \mu X) + BR(B \to DX)\, BR(D \to \mu X)] \simeq 0.18$. Barate et al. quote $\sigma_B \cdot BR(B \to \psi K\pi) = 2$ nb. This implies $\sigma_{B\bar{B}} BR(B\bar{B} \to \psi\mu) \cdot BR(\psi \to \mu\mu) = 90$ pb (using $BR(\psi \to \mu\mu) = 0.07$), for 150 GeV π^-, which is considerably larger than the measurements (see Table VII) of (-8 ± 12) pb and (22 ± 22) pb for 400 GeV protons.

In the analysis it was assumed for simplicity that the charged and neutral states have equal semileptonic branching ratio of 10%. We have assumed 10% rather than the free quark model value of 14% to account for some enhancement of the hadronic modes. The ψμ signature is sensitive only to the average semileptonic BR of the B^o and B^+. It is even less sensitive because some of the extra muons come from the final state D decay. However, if the muonic branching ratio of the B^+ is greater than that of the B^o in analogy with the recently observed[20,21,22] difference between D^+ and D^o branching ratios, then the 3μ final states would be suppressed and the $\mu^+\mu^+$ final states would be slightly enhanced due to the sign correlation between B and D in the cascade decays. A difference between the B^o and B^+ branching ratio is not unexpected in view of recent theoretical investigations[24] of the reasons for the D^o, D^+ lifetime difference.

V. CONCLUSIONS

The experimental evidence for prompt single muons, prompt neutrinos and prompt dimuons with missing energy indicates that about 30% of prompt muons come from single sources in 400 GeV p-Fe collisions. The data indicates that the source of such single leptons is a particle with a semileptonic branching ratio of ∿5% and with a hadronic production cross section of ∿20 nb. Charm production is the most likely explanation since all other known lepton sources are ruled out.

A charm cross section of 20 μb is smaller than the 170 μb predicted by gluon vector dominance models[51]. It is somewhat larger than the few μb originally predicted by QCD calculations[63]. It can accomodated within QCD models if the effective mass of the charm quark is taken to be[56] about 1.3 GeV rather than 1.8 GeV. It may also be accomodated if non-perturbative diagrams are included.[55]

The multimuon final states can be studied to look for bottom particle production signatures. Limits of 40 nb per nucleon are obtained from the data. These are smaller than the 850 nb predicted by gluon vector dominance models[51] but are consistent with the 10 nb obtained from QCD calculations.[55] The 40 nb limit for 400 GeV pp interaction is smaller than the 200 nb indicated by recent reports[15] of a peak in the $\psi K\pi$ mass spectrum for 150 GeV $\pi^- N$ collisions.

The backgrounds in the multimuon signature are small (if p_t and missing energy cuts are applied). This indicates that with additional data a signal of the order of 10 nb (predicted by QCD) may be observable.

The measurement of hadronic production cross sections for heavy quark final states (i.e. charm, bottom) is important theoretically. It is very rare that hadronic cross sections can be calculated theoretically. However, QCD calculations of the production cross section of charm and bottom states are more feasible because of the heavy mass of the final state quarks. These calculations involve both q-$\bar{q}$ and gluon processes. Therefore, the measurement of charm and bottom cross sections provide information on quark and gluon distributions. In this sense, these measurements compliment Drell-Yan and deep inelastic experiments which yield information mostly on quark distributions within the nucleon.

APPENDIX I SOURCES OF NON-PROMPT LEPTONS

The backgrounds to prompt lepton experiments originate from long lived states. Aside from the conversion of real photons to e^+e^- and $\mu^+\mu^-$ pairs, all other non-prompt sources such as π,k decays, yield single leptons in the final state (aside from uncorrelated double π decays).

AI.1 Non-linearities (muons)

Table VIII shows the sources of non-prompt muons. These are dominated by the π and k decay contribution. These backgrounds are eliminated using the density extrapolation method. For a particle of lifetime $c\tau$ the decay length in the laboratory system is $\Lambda d = c\tau\gamma$ where $\gamma = E/M$. The interaction length in steel Λ_i is about 20 cm.

The muon decay rate from any particle as a function of density is

$$R(\rho) = \sigma \times (BR) \times \frac{\Lambda_i}{\Lambda_d} \frac{\rho_{Fe}}{\rho} \left[\frac{1}{1 + \left(\frac{\Lambda_i}{\Lambda_d}\right)\left(\frac{\rho_{Fe}}{\rho}\right)} \right]$$

where σ is the production cross section for π,K etc. and BR is the branching ratio to muons. The dependence on $1/\rho$ is exactly linear in the limit $\Lambda_i/\Lambda_d \to 0$.

Table 9 shows the ratio for all non prompt muon sources with a typical lab energy necessary to yield 8 GeV muon. As can be seen, the non-linear term is very small for π's and K's which dominate the non-prompt muon rate. For the hyperons, the non linear term is somewhat larger, but the hyperon branching ratios to muons is small and the production cross sections for high energy hyperons is also small[57]. The hyperons must be high energy in order that their 3 body decay yield an 8 GeV muon.

AI.2 Fake Intercept (muons)

In addition to small non-linearity arising from the finite lifetime of pions and kaons, there is an additional fake signal which arises from the fact that the density is non uniform. The target is composed from steel plates with air gaps. Pions attenuate in the steel plates before they reach the gaps. A simple calculation yields a fake signal which is a fraction $1/12(\ell/\Lambda_i)^2$ of the π,K decay. Here $\Lambda_i \simeq 20$ cm is the π,K interaction length and ℓ is the plate thickness. In a typical experiment[9,10] $\ell \simeq 3.8$ cm. So the fake signal is 0.3% of the π,K decay contribution (i.e. very small).

In addition, there could be a non prompt intercept due to decays occurring in non-expanded regions, i.e. upstream and downstream interactions. This has been discussed in the text.

AI.3 Non-direct Electron and Non-prompt ν Sources

The background for direct electron experiment are e^+e^- pairs from real photon conversions and Dalitz decays (see Table III). In addition, there are electron sources that come from long lived sources. These must be calculated and subtracted. They are important in beam dump experiments[11] [see H. Wachsmuth CERN/EP 79-125 (1979)]. These are listed in Table 10. The Ke3 and the Σ^- decays are most important.

APPENDIX II SOURCES OF PROMPT DILEPTONS

This will only be a brief summary since dileptons have already been reviewed by Smith at this Conference. The dilepton spectrum consists of a continuum plus resonances.

1. The resonance contributions tend to follow a scaling law. The scaling function $F_R(\tau)$ is similar to that of Drell-Yan production, but is not identical to the Drell-Yan function because gluon-gluon processes contribute also. Each resonance (listed in Table II e.g. $\rho,\omega,\phi,\psi,\psi',\Upsilon$ etc.) cross section could be described[55] as

$$\left(\frac{d\sigma}{dM_{\mu\mu}}\right)_R = A(M_{\mu\mu}-M_R)\,\frac{F_R(\tau)}{M_R^3}\,\Gamma_R(\mu\mu)$$

where M_R is the resonance mass, $\tau=M_R^2/S$, $\Gamma_R(\mu\mu)$ is the leptonic width, S is the square of the center of mass energy, $F_R(\tau)$ is a universal function for the resonances and $A(M_{\mu\mu}-M_R)$ is the resonance shape (i.e. a Breit-Wigner).

2. The high mass continuum ($M_{\mu\mu}>4$ GeV) is described by the contribution of initial state quark-antiquark annihilation Drell-Yan processes, i.e.

$$\frac{d\sigma}{dM_{\mu\mu}} = \frac{F'_{DY}(\tau,M_{\mu\mu})}{M^3_{\mu\mu}}$$

where $F'(\tau,M_{\mu\mu})$ is related to the target and projectile structure functions. The scaling violations (i.e. $F'(\tau,M_{\mu\mu})$ not a function of τ only) at high energies are small for p-p collisions[6]. For π^-N collisions[7,8] there is a question of a normalization[8] factor of 1.5 to 2.0 between data and theory or a possible A dependence problem. The normalization problem may be related[62] to second order QCD (see review by Smith, this Conference).

3. In addition to the Drell-Yan continuum, there is a hadronic source of dimuons at low masses $1<M_{\mu\mu}<1$ GeV. One interpretation of this contribution is that it is due to <u>final state</u> quark-antiquark annihilation of $q\bar{q}$ pairs which have been hadronically produced. The Rochester-NSF-BNL collaboration has extracted[59] the ratio of this contribution to the Drell-Yan contribution by looking at the ratio of π^+N and π^-N dimuon cross sections. For $1<M_{\mu\mu}<4$ GeV they obtain

$$\frac{d\sigma}{dM_{\mu\mu}} = \left.\frac{d\sigma}{dM_{\mu\mu}}\right|_{DY} \times \frac{1}{\gamma(M_{\mu\mu})}$$

where $\gamma(M_{\mu\mu}) \to 1$ for $M_{\mu\mu}\to 4$ GeV. This ratio would be target mass dependent. This is because the Drell-Yan pairs have an $A^{1.0}$ target mass dependent and the hadronic $\mu\mu$ pairs have an $A^{2/3}$ dependence. This may be the reason why the A dependence of $\mu\mu$ pairs changes from $A^{2/3}$ at low $M_{\mu\mu}$ to $A^{1.0}$ at high $M_{\mu\mu}$. The dependence of $\gamma(M_{\mu\mu})$ on $M_{\mu\mu}$ for a Cu target[59] is shown in Fig. 10.

4. There is some uncertainty about the magnitude of the scaling violations in dimuon production. The p-p data indicates small scaling violations[5]. This is expected because the high energy data has rather limited Q^2 range and accurate lower energy pp data is not available. Scaling violations in p-p dimuon production are expected to be small because most of the contribution to the cross section is from the antiquarks in the low X region where the scaling violations are not large. On the other hand, π^-N collisions involve antiquarks at large X where the structure function exhibit large scaling violations. A comparison of the π^- structure functions extracted from low energy BNL data[9] with higher energy data shows agreement with the QCD predictions[9,61]. This agreement must be viewed with caution because the high energy data has the normalization uncertainty of 1.5

to 2.0. Also, the extraction of the structure functions from low energy data involve the previously discussed correction for non Drell-Yan hadronically produced pairs. This hadronic contribution is subtracted before the structure functions are extracted from the low energy data.

5. The mean p_T of $\mu^+\mu^-$ pairs is large at high energies, possibly due to gluon corrections. There are attempts to extract the primodial p_T distribution of the quarks from lower energy $\mu^+\mu^-$ data[60] where the gluon contribution is expected to be smaller.

6. At very low masses $M_{\mu\mu} < 1$ GeV, there are large Dalitz decay contributions in addition to the Drell-Yan and the $\mu^+\mu^-$ pairs of hadronic origin. Since this region is dominated by non Drell-Yan pairs, the A dependence is about $A^{2/3}$.

RECORD OF QUESTIONS

Name: M. S. Tannenbaum, Rockefeller University

I'd like to comment on the ISR single electron data. There are 2 experiments, CCRS at 90° (Busser et al), and Baum et al 30°. For the CCRS experiments, we vetoed on π^0 Dalitz decay and also tried to measure low mass e^+e^- pairs with μ_{ee}>400 MeV/c^2. We concluded that the single electrons could not be explained by a low mass e^+e^- continuum unless the mass dependence was M^{-1} or flatter. A continuum falling like 1/M could occur from Dalitz decay or real single photon production, and a γ/π^0 ratio of ∿10% for p_T>1.3 GeV/c could have explained the single lepton signal. However subsequent experiments showed that γ/π^0 in this p_T range was $\lesssim$1%, thus ruling out this production mechanism. The fact that part of this single e signal might be explained by charm was first discussed by Boorquin and Gaillard and by Hinchliff and Llewelyn Smith.

Bodek: I agree, the CCRS data and the Fermilab data are both consistent with a significant charm contribution

Name: Neville W. Reay, Ohio State University

You ran with 400 GeV protons on target, Goliath ran with 165 GeV pions on target. Near threshold, the rise of pion and proton production cross-sections are considerably different. Can you comment on how you expect your limits on $B\bar{B}$ production should compare with the Goliath signal on $B\bar{B}$ production?

Bodek: As I discussed in the talk, gluon-vector-dominance model predict a larger cross section for 400 GeV pp than for 150 GeV π^-p (850 nb vs. 200 nb). Our data is not consistent with that. On the other hand if $q\bar{q}$ processes are important, pions would be more effective. For example, the ratio of Υ production cross section for 150 GeV π^-p to Υ production by 400 GeV protons is only 2±1.4. Therefore, our limit of 40 nb as compared to Goliath's 200 nb is about 2σ from that ratio. This indicates the need to do $B\bar{B}$ searches and multimuon experiments with pion beams.

Name: Jack Sandweiss, Yale University

1. How many pions of energy greater than 150 GeV are produced by the proton interactions in your experiment?

2. How sensitive are your limits on the $B\bar{B}$ production cross sections to the assumed branching ratios for the B system?

Bodek: 1. Each proton interaction produces secondary protons and pions which reinteract. We have not subtracted the contribution of these secondary interaction from our $B\bar{B}$ limits. However, there are many more secondary protons with E>150 GeV than secondary pions.For each incident proton there are 0.4 secondary and tertiary protons with E>150 GeV and only 0.018 secondary and tertiary pions ($\pi^+ + \pi^-$).

2. As discussed in the text, our sensitivity to the semi-leptonic branching ratio of the B particles affects the conclusion from the ψ_μ data in less than a proportional dependence. We assume that the $B \to X_{\mu\nu}$ branching ratio is 10% and the $B \to D \to X_{\mu\nu}$ is 8%. If the $B \to X_{\mu\nu}$ branching ratio were 5% then our limit would increase by less than a factor of 2. The limits from the 3μ and $\mu^+\mu^-$ final state are more sensitive to the difference between the $B^o B^+$, D^o and D^+ branching ratios due to the sign conditions in the cascade decays. If the B^o semileptonic branching ratio was smaller than the B^+ then the 3μ final states would be suppressed and the $\mu^+\mu^+$ final state would be slightly enhanced.

REFERENCES

1. L. M. Lederman, Physics Reports C, 1976 (149-181).
2. N. S. Craigie, Physics Reports 47, 1978 (1-148).
3. J. E. Augustin et al., Phys. Rev. Lett. 33, 1406 (1974).
4. J. J. Aubert et al., Phys. Rev. Lett. 33, 1404 (1974).
5. S. Herb et al., Phys. Rev. Lett. 39, 252 (1977).
6. J. A. Appel et al., Phys. Rev. Lett. 40, 435 (1978).
7. C. B. Newman et al., Phys. Rev. Lett. 25, 1523 (1970) (Chicago-Princeton collaboration).
8. J. Bodier et al., EPS Intern. Conf. on High Energy Physics (Geneva 1979); R. Barate et al., Phys. Rev. Lett. 43, 1541 (1979).
   D. McCal et al., Phys. Lett. 85B, 432 (1978) (Rochester-NSF-BNL collaboration).
9. K. W. Brown et al., Phys. Rev. Lett. 43, 410 (1979)(Caltech-Stanford collaboration).
10. J. Ritchie et al., Rochester Preprint UR-717 (Oct. 1979) "Prompt Muon Production at Small X_F and P_T in 350 GeV p-Fe Collisions" [Caltech-Fermilab-Rochester- Stanford collaboration].
11. P. C. Boseti et al., Phys. Lett. 74B, 143 (1973); P. Alibran et al., ibid 134, T. Hansl et al., ibid 139; for more recent results see H. Wachsmuth, Invited talk - Lepton Photon Conference, Batavia, 1979, also available as CERN-EP/79-115 Oct. 1979 and H. Wachsmuth CERN/EP 79-125, Oct. 1979. See also Ref. 50.

12. A. M. Diament-Berger et al. Phys.Rev.Lett. 43, 1774 (1979).
13. A. M. Diamant-Berger et al., "Search for Possible Signatures of Bottom-Quark States Produced in 400 GeV p-Fe Interactions."
14. Fermilab proposal E595, Caltech-Fermilab-Rochester-Stanford Collaboration, A. Bodek, spokesman.
15. R. Barate et al., "Possible Observation of a New Meson at 5.3 GeV." Paper #184, submitted to the International Photon and Lepton Conference, Batavia, IL. 1979.
16. "An Experiment to Observe Directly Beauty Particles Selected by Muonic Decay in Emulsion" CERN Proposal #223 PPESP/79/41 (Oct. 1979) P. Musset, spokesman.Bori, Brussels, CERN, UC Dublin, UC London, Open University, Rome, Turin collaboration.
17. A.J.S. Smith, "Lepton Pair Production in Hadronic Collisions", this conference.
18. K. J. Anderson et al., Phys. Rev. Lett. 37, 803 (1976).
19. J. P. Boymond et al., Phys. Rev. Lett. 33, 112 (1974).
20. N. W. Reay, this conference.
21. J. Kirkby, Invited talk, Lepton-Photon Conference, Batavia, IL. (1979) (DELCO results).
22. J. Dorfan, this conference (Mark II results).
23. J. L. Rosner, Proceedings of the Cosmic Ray and Particle Physics-1978 (Bartol Conference) p. 297, T. K. Gaisser editor.
24. K. Jagannathan and V. S. Mathur, Rochester preprint UR-728 (Oct. 1979).
25. H. Fritzsch, Physics Letters 80B, 343 (1979).
26. C. Bricman, "Review of Particle Properties" Phys. Lett. 75B, 1 (1978).
27. H. Meyer, Invited talk, Lepton-Photon Conference, Batavia, IL. 1979.
28. Yu. B. Bushnia et al., Phys. Lett. 79B, 147 (1978); R. I. Dzhelyadin, Phys. Lett. 84B, 143 (1979); R. I. Dzhelyadin et al., IFVE 79-121.
29. C. H. Lai and C. Quigg, Fermilab FN-296 (Sept. 1976); N. S. Craigie and D. Schildknecht, Nucl. Phys. B118, 311 (1977), C. Quigg and J. Jackson, UCRL 18487 (1968).
30. B. C. Barish et al., IEEE, Transactions on Nuclear Science, BS25, No. 1, p. 532 (Feb. 1978).
31. The range detector consists of half of the neutrino target used in Lab E neutrino experiments. (E356, E616 Caltech-Fermilab-Rochester-Rockefeller).
32. The accidental 2μ rate originates from uncorrelated decays of two pions. It is determined from the square of the single muon rate at each density and subtracted.
33. F. E. Taylor, et al., Phys. Rev. D14, 1217 (1976).
34. The parametrization used was $\mu/\pi = A(s)B(X_F)\times10^{-4}$, with $A(s)=(-1.91+0.88\ \ln\sqrt{s})$ for $\sqrt{s}>15.44$, $A(s)=0.5$ for $\sqrt{s}<15.44$, and $B(X_F)=(1-2X_F)$ for $X_F>0.4$ and $B(X_F)=(1-X_F)/3$ for $0.4<X_F<1.0$. This form was used with the hadron spectra from secondary and tertiary interactions and yielded a contribution of 1.22×10^{-4} prompt muons per interaction. An additional contribution of

0.38×10^{-4} from photon conversions was calculated using π^0 spectra.

35. The shower calculation correctly predicted the observed non-prompt muon rate of 18×10^{-4} per interaction in the compacted configuration. A contribution of 7.2×10^{-4} per interaction comes from the decay of 3.55 pions and 0.39 kaons (with $P_\pi>8$ GeV) produced in the primary collision. An additional 10.5×10^{-4} originates from the 2.7 pions and 0.3 kaons produced in secondary and tertiary collisions.

36. The upper limit is obtained by dividing the prompt μ rate from all generations (primaries, secondaries and tertiaries) by the 3.55 primary π's only. The lower limit is obtained by assuming the $\sqrt{s}$ dependence of μ/π is flat (i.e., same for primaries and secondaries). The prompt μ rate from all generations is then divided by the 6.25 π's from all generations.

37. J. G. Branson et al., Phys. Rev. Lett. 38, 457 (1977), these authors have also expressed the results of H. Kasha et al., Phys. Rev. Lett. 36, 1007 (1976), on μ^+/π^+ and μ^-/π^- in terms of $\mu^++\mu^-/\pi^++\pi^-$ using π^+/π^- data; K.W.B. Merritt et al., (to be published). Preliminary data presented by M.H.Shaevitz in Proceedings of the 3rd International Conference on New Results in High Energy Physics, Vanderbilt (1978) p. 138.

38. A 10% correction has been applied yielding $\mu/\pi=(1.03\pm0.14)\times10^{-4}$ at $X_F=0.03$. The value of 0.93×10^{-4} is an average over the forward hemisphere and includes contribution from larger value of X_F (Fig. 2).

39. M. Barone et al., Nucl. Phys. B132, 29 (1978);L. Baum et al., Phys. Lett. 60B, 485 (1976).

40. An average value of 4.0×10^{-4} was obtained by taking a fit to the ISR data (Fig. 4a) $e/\pi=1.42\times10^{-4}$ for P_T 1.06 GeV, $e/\pi=(1.5/P_T)\times10^{-4}$ for $0.25\leq P_T\leq1.06$ and $e/\pi=6.0\times10^{-4}$ for $P_T\leq0.25$ GeV, and folding it against the P_T spectrum of pions with $P_\pi>8$ GeV. The range of (3.2 to 4.8)$\times10^{-4}$ is obtained by using extreme assumptions about the behavior of e/π for $P_T<0.2$ (i.e. the three curves shown in Fig. 4a).

41. F. W. Busser et al., Nucl. Phys. B113, 189 (1976).

42. J. G. Branson et al., Phys. Rev. Lett. 38, 1334 (1977).

43. E. W. Beier et al., Phys. Rev. Lett. 37, 1117 (1976).

44. J. Ballam et al., Phys. Rev. Lett. 41, 1207 (1978); Y. Makdisi et al., Phys. Rev. Lett. 41, 367 (1978).

45. L. Baum et al., Phys. Lett. 77B, 337 (1978); 68B, 279 (1977).

46. Large charm baryon cross sections have been reported by ISR experiments (see A.Kernan, Lepton-Photon Conference, Batavia 1979 and ref. 47) but these measurements are at large X_F as compared to the small X_F of Ref. 39.

47. K. L. Giboni et al., Phys. Lett. 85B, 437 (1979); W. Lockman et al., ibid 443; D. Drijard et al., 85B, 452 (1979).

48. W. M. Geist, CERN/EP 79-78 (July 1979).

49. E. Amaldi et al., Nucl. Phys. B158, 1 (1979).

50. H. Wachsmuth, Proceedings of the Topical Conference on Neutrino Physics, Oxford, July 197 , p. 233, A. G. Michette, P. B. Renton, editors.

51. H. Fritzsch and K. H. Streng, Phys. Lett. 78B, 447 (1978).
52. J. Badier et al., Phys. Lett. 86B, 98 (1979).
53. D. Garelick et al., Phys. Rev. D18, 945 (1978); J. K. Yoh et al., Phys. Rev. Lett. 41, 684 (1978).
54. E. J. Siskind et al., CALT-68-665 (1979) to be published in Phys. Rev. D.
55. F. Halzen, Proceedings of the Cosmic Ray and Particle Physics-1978 (Bartol Conference) Delaware, p. 261, T. K. Gaiser,ed.).
56. C. Carlson and R. Suaya, SLAC PUB 2212 (71).
57. H. Kichimi et al., Phys. Lett. 72B, 411 (1978); M. Bourquin et al., Nucl. Phys. B153, 13 (1979); K. Doroba, Fermilab TM-818 (1979).
58. D. A. Dicus and J. R. Letaw, ORO 3992-368 Aug. 1979, Univ. of Texas, Austin preprint (Leptonic decays of the Ω^-).
59. C. Reece et al., Phys. Lett. 85B, 427 (1979); D.McCal et al., Phys. Lett. 43, 410 (1978), (Rochester-BNL-NSF collaboration).
60. W. J. Metcalf et al., Rochester preprint UR-726 (1979).
61. A. Donnachie and P.V. Landshoff, Nucl. Phys. B112, 233 (1976).
62. J. Ellis, invited talk, Lepton-Photon Conference, Batavia, Oct. 1979 (available as Ref. TH.2744-CERN).
63. J. Babcock, D. Sivers, S. Wolfram, Phys. Rev. D18, 162 (1978).

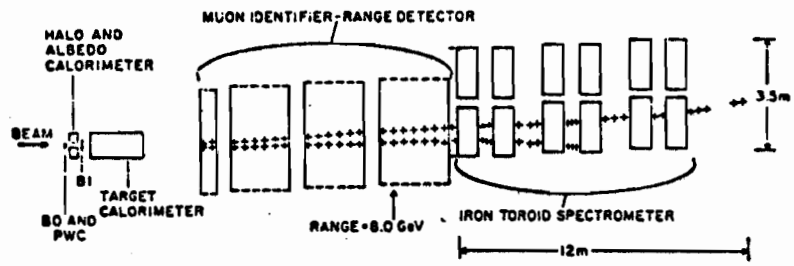

Fig. 1 Plan view of the Caltech-Fermilab-Rochester-Stanford apparatus. The beam is incident from the left. A dimuon event is shown to illustrate the spark chamber locations. In addition to the 22 3m×3m spark chambers, the 360 ton range detector contains 42 3m×3m scintillation counters. (Ref. 10.)

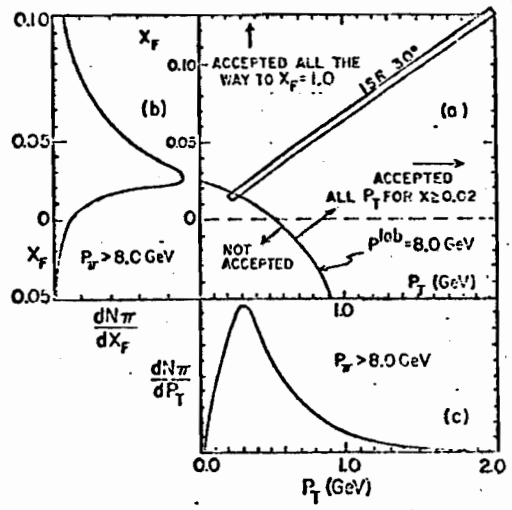

Fig. 2 The acceptance of the Caltech-Fermilab-Rochester-Stanford experiment covers almost the entire forward hemisphere in the center of mass, except for a small region around the point X_F=0,P_T=0. The region covered by the ISR 30° direct electron experiment is shown for comparison. A calculated spectrum of pions produced in 350 GeV P-Fe interactions with P_π > 8 GeV is shown versus X_F and P_T.(Ref. 10.)

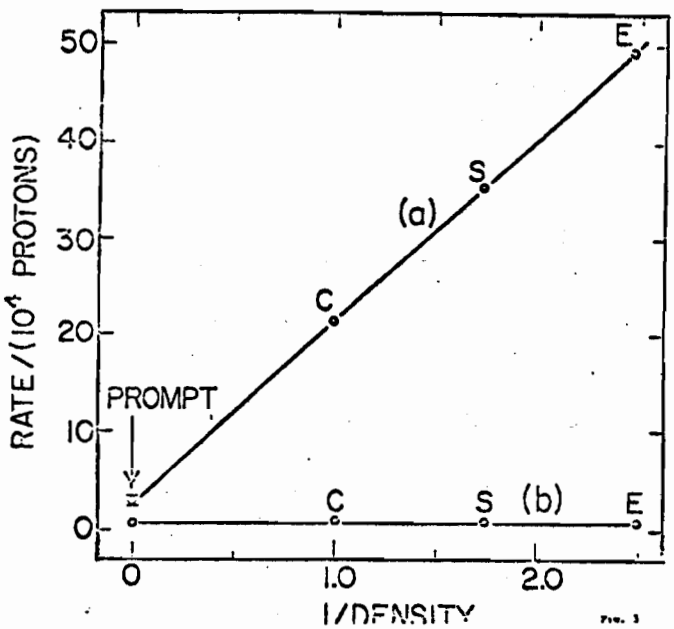

Fig. 3 The event rates versus inverse density. (Caltech-Fermilab-Rochester-Stanford) The extrapolated rate is the prompt signal. (a) events with at least one muon with $P_\mu > 8$ GeV; (b) events with two muons each with $P_\mu > 8$ GeV. (Ref. 10.)

Fig. 4 The μ/π ratio measured in the Caltech-Fermilab-Rochester-Stanford experiment (p-Fe at 350 GeV) compared to (a) ISR p-p direct electron data at small X_F vs. P_T (Refs.39 and 41), and (b) prompt muon data at small P_T vs. X_F (Ref. 37). The data of Kasha et al. (p-Cu) is at 400 GeV and of Branson et al. (p-Fe) is at 200 GeV. The experiment of K.W.B. Merritt et al. (p-Fe, 400 GeV) was performed using an earlier version of our apparatus.

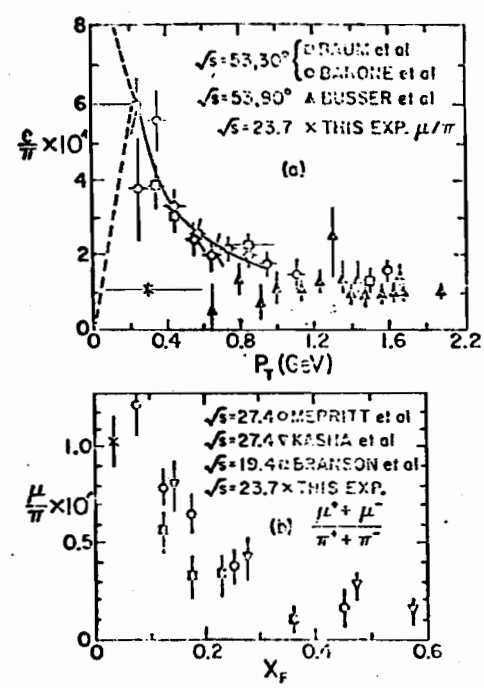

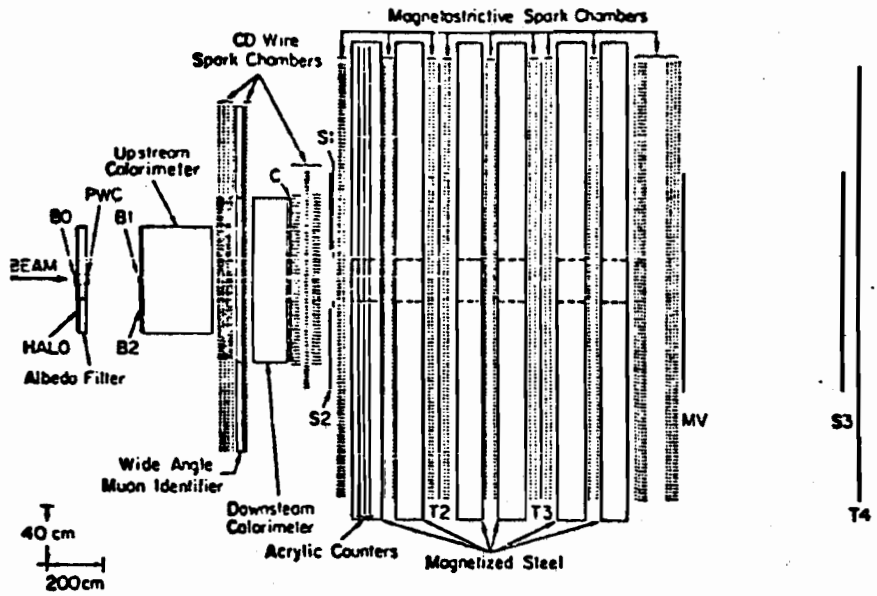

Fig. 5 The Caltech-Stanford apparatus for detection of prompt muons at high P_T. The toroidal geometry of the magnets is used to trigger on high P_T muons by requiring muons to remain in the same toroid quadrant (Ref. 9).

Fig. 6 Prompt single μ rate and 2μ rate versus inverse density for muon with $P_T \gtrsim 0.8$ GeV (Caltech-Stanford, Ref. 9).

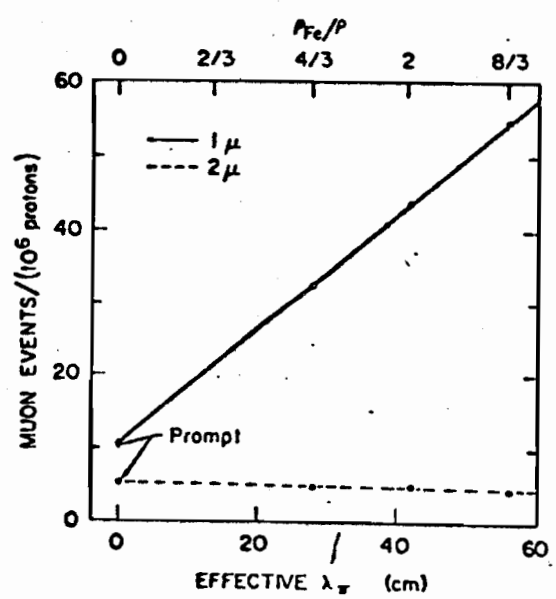

Fig. 7 The total observed energy $E_{\mu^-}+E_{\mu^-}+E_{calorimeter}$ for opposite sign dimuon events. Events with large missing energy originate from double weak decays of charm states (Caltech-Stanford, Ref. 12). The dashed line is a fit to data taken simultaneously for unbiased proton interactions in the calorimeter (i.e. without any muon requirements).

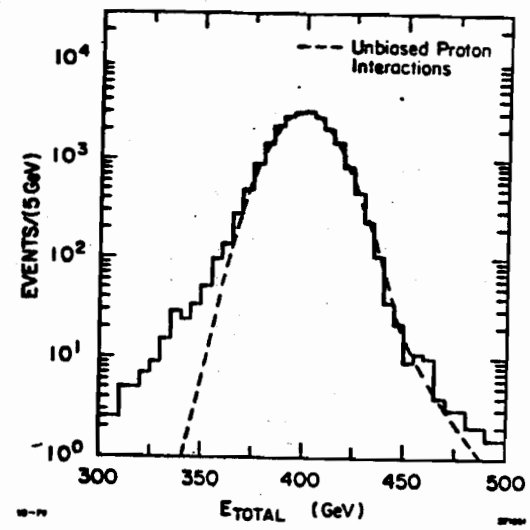

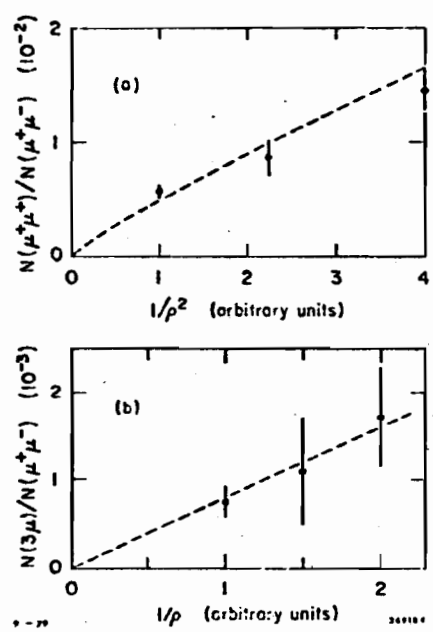

Fig. 8 Multimuon rates versus inverse density $(1/\rho)$ (Caltech-Stanford, Ref. 13).
a) $\mu^+\mu^+/\mu^-\mu^-$ events vs. $1/\rho^2$. The curve is the expected distribution if all same sign events were due to a single muon (from charm or π decay) with an additional accidental π decay muon.
b) $3\mu/\mu^+\mu^-$ vs. $1/\rho$. The curve is the expected distribution if all the events were due to a $\mu^+\mu^-$ pairs from electromagnetic sources accompanied by an additional accidental π decay muon.

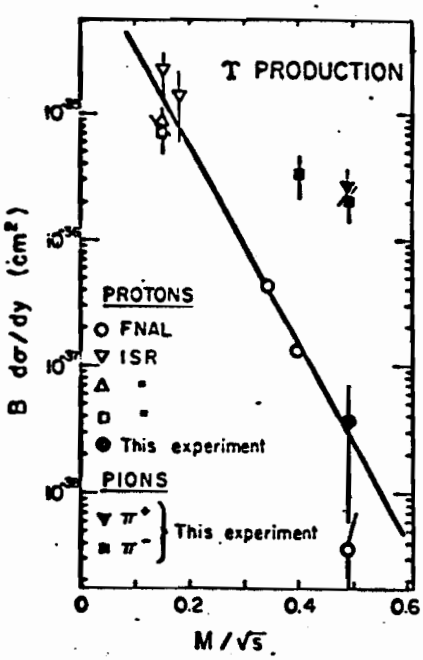

Fig. 9 Υ production cross section for protons and pions (Ref. 52).

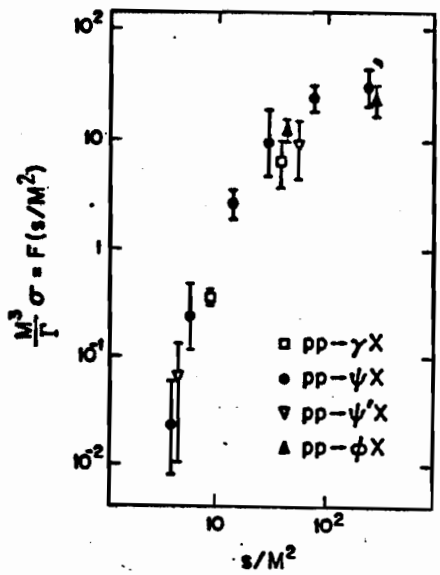

Fig. 10 The figure demonstrates that the quantity $m^3/\Gamma\text{-}\sigma$ is a universal function of s/m^2 for different flavor bound states. m, Γ and σ are respectively the mass, direct hadronic width and production cross section of the flavor bound state (Ref. 55).

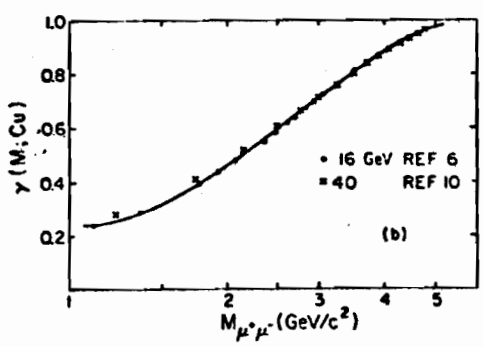

Fig. 11 The fraction of Drell-Yan $\mu^+\mu^-$ pairs for a Cu target as a function of the $\mu^+\mu^-$ mass. (Rochester-BNL-NSF, Ref. 59)

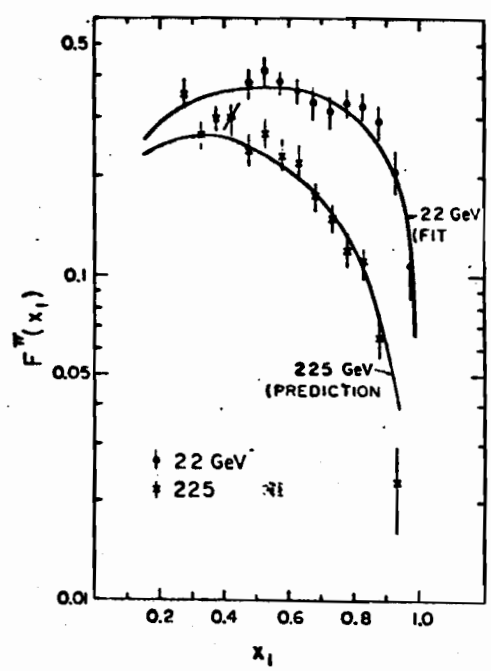

Fig. 12 Pion structure function extracted from low and high energy data (Rochester-BNL-NSF, Ref. 59 and Chicago-Princeton, Ref. 7).

Table 1: Sources of prompt leptons from weak decays. These yield mostly single leptons with equal branching ratios to $X_{\mu\nu}$ and $X_{e\nu}$ final states. If experimental values are not available theoretical estimates are given (TH). As is indicated all have $C\tau \ll 1$ cm. Charm lifetimes are from Ref. 20; semileptonic branching ratios are from Ref. 21,22 and theoretical estimates are from References 23,24,25.

Particle	Lifetime	Decay Mode	Branching Ratio
Charm:			
$D^{\pm}$	$(9.3\pm5.2)\times10^{-13}$sec $C\tau\simeq3\times10^{-2}$ cm	$K(K^*)\mu\nu$	$\begin{cases}15.8\pm5.3\% \\ 23\pm6\ \%\end{cases}$
D^o	$(0.66\pm0.4)\times10^{-13}$sec $C\tau\simeq2\times10^{-3}$ cm	$K(K^*\mu\nu)$	$(5.2\pm3.3)\%$ $<4\%$
$F^{\pm}$	$(2\pm1)\times10^{-13}$sec $C\tau\simeq6\times10^{-3}$ cm	$X_{\mu\nu}$	$\begin{cases}=D^o\ (TH) \\ = BR(D^+)\ \frac{\tau_F}{\tau_{D^+}}\ (TH)\end{cases}$
		$\tau^{\pm}\nu_{\tau}$	$(1.9\pm1.6)\%$ (TH)
Λ_C	$(0.55\pm0.33)\times10^{-13}$sec $C\tau\simeq1.6\times10^{-3}$cm $(2$ to $4)\times10^{-13}$sec (TH)	$\Lambda_C X_{\mu\nu}$	seen in ν interactions $= BR(D^+)\ \frac{\tau_\Lambda}{\tau_{D^+}}$ (TH)
$\tau^{\pm}$	2.9×10^{-13}sec (TH) $C\tau\simeq9\times10^{-3}$cm		$(17.5\pm1.7)\%$
Bottom			
$B^{\pm},B^o$	$\tau_B>1.3\times10^{-15}$sec (TH) $C\tau>4\times10^{-5}$cm	$D(D^*)\mu\nu$ DX $\llcorner\ \mu\nu$ ψX $\llcorner\ \mu^+\mu^-$	$\sim10\%$ (TH) 100% (TH) $\llcorner\!\to 8\%$ 3% (TH) $\llcorner\!\to 7\%$

Table 2: Electromagnetic sources of prompt dileptons which are expected to have equal branching ratio to e^+e^- and $\mu^+\mu^-$ pairs (note $\Gamma = 1$ ev $\Rightarrow \tau \simeq 10^{-15}$ sec). Most data is from ref. 26. Data on the Υ family is from ref. 27.

Particle	Γ, Full width (MeV)	BR to (e^+e^- or $\mu^+\mu^-$)
γ_v virtual photon	(for $m_{\mu\mu} \gtrsim 4m_\mu$)	($e^+e^- = \mu^+\mu^-$ away from $2m_\mu$ threshold)
$\eta(549)$	(0.85 ± 0.12) KeV	$(2.2 \pm 0.8) \times 10^{-5}$
$\rho(770)$	(155 ± 3) MeV	$(4.3 \pm 0.5) \times 10^{-5}$
$\omega(783)$	(10.1 ± 0.3) MeV	$(7.6 \pm 1.7) \times 10^{-5}$
$\phi(1020)$	(4.1 ± 0.2) MeV	$(3.1 \pm 0.1) \times 10^{-4}$
$\psi(3100)$	(67 ± 12) KeV	$(7 \pm 1)\%$
$\psi'(3685)$	(228 ± 56) KeV	$(0.9 \pm 0.1)\%$
$\psi''(3772)$	(28 ± 5) MeV	$(1.3 \pm 0.2) \times 10^{-5}$
$\psi''(4415)$	(33 ± 10) MeV	$(1.3 \pm 0.3) \times 10^{-5}$
$\Upsilon(9460)$	$\Gamma_t \simeq 57$ KeV, $\Gamma_e \simeq (1.35 \pm 0.14)$ KeV	$(2.3 \pm 1.4)\%$
$\Upsilon'(10010)$	$\Gamma_t \simeq$? , $\Gamma_e = (0.32 \pm 0.13)$ KeV	seen
$\Upsilon''(10410)$	$\Gamma_t \simeq$? , $\Gamma_e = 2/3\ \Gamma_e(\gamma')$	seen

Table 3: Short lived electromagnetic sources of lepton pairs that have different branching ratios for electrons and muons. Muons from such sources are typically not subtracted in prompt muon experiments but must be subtracted in direct electron experiments because π^o and η Dalitz decays dominate the measured electron spectra. Branching ratios are from ref. 26 and ref. 28. Wherever branching ratios measurements are not available I have inserted theoretical estimates from ref. 29 (TH) or rough estimates (RE) using $BR(Xee)/BR(X\gamma)\approx 10^{-2}$ and $BR(X\mu\mu)/BR(X\gamma)\approx 10^{-3}$.

Source	Decay Mode	BR
γ_v(virtual photon)	$2m_e < m_{ee} < 4m_{\mu\mu}$	μ,e difference due to threshold factors
$\pi_o(135)$	$\gamma\gamma$	$(98.85\pm0.05)\%$
	e^+e^- $\gamma\, e^+e^-$	$(1.15\pm0.05)\%$
	e^+e^- $e^+e^-e^+e^-$	3.32×10^{-5}
$\eta(549)$	$\gamma\gamma$	$(38\pm1)\%$
	$\pi^+\pi^-\gamma$	$(4.89\pm0.13)\%$
	$\pi^o\gamma^-\gamma$	$(3.1\pm1.1)\%$
	e^+e^- $\gamma\, e^+e^-$	$(0.50\pm0.12)\%$
	e^+e^- $\pi^+\pi^-e^+e^-$	$(0.1\pm0.1)\%$
	e^+e^- $\pi^o\gamma\, e^+e^-$	$\sim 3\times10^{-4}$ (RE)
	$\mu\,\mu$ $\gamma\,\mu^+\mu^-$	$(1.5\pm0.75)\times10^{-4}$
	$\mu\,\mu$ $\pi^+\pi^-\mu^+\mu^-$	$\sim 5\times10^{-5}$ (RE)
	$\mu\,\mu$ $\pi^o\gamma\,\mu^+\mu^-$	$\sim 3\times10^{-5}$ (RE)
$\rho(770)$	$\pi^o\gamma$	$(2.4\pm0.7)\times10^{-4}$
	$\pi^o\, e^+e^-$	$\sim 2.4\times10^{-6}$ (RE)
	$\pi^o\,\mu^+\mu^-$	$\sim 2.4\times10^{-7}$ (RE)
$\omega(738)$	$\pi^o\,\gamma$	$(8.8\pm0.5)\%$
	$\pi^o\, e^+e^-$	8×10^{-4} (TH)
	$\pi^o\,\mu^+\mu^-$	$(9\pm5)\times10^{-5}$

Table 3 (continued)

Source		Decay Mode	BR	
$\phi(1020)$		$\eta\,\gamma$	$(1.6 \pm 0.6)\%$	
		$\pi^o\gamma$	$(0.14 \pm 0.05)\%$	
	e^+e^-	$\eta\, e^+e^-$	1.7×10^{-4}	(TH)
		$\pi^o e^+e^-$	1.25×10^{-5}	(TH)
	$\mu^+\mu^-$	$\eta\, \mu^+\mu^-$	6.7×10^{-6}	(TH)
		$\pi^o\mu^+\mu^-$	1.25×10^{-6}	(TH)
$\eta'(958)$		$\rho^o\,\gamma$	$(29.8 \pm 1.7)\%$	
		$\omega\,\gamma$	$(2.1 \times 0.4)\%$	
		$\gamma\,\gamma$	$2.0 \times 0.3\ \%$	
	e^+e^-	$\rho\, e^+e^-$	2×10^{-3}	(TH)
		$\omega\, e^+e^-$	$\sim 2 \times 10^{-4}$	(RE)
		$\gamma\, e^+e^-$	3.6×10^{-4}	(TH)
	$\mu^+\mu^-$	$\rho\, \mu^+\mu^-$	3×10^{-4}	(RE)
		$\omega\, \mu\, \mu$	2×10^{-5}	(RE)
		$\gamma\, \mu\, \mu$	$(8 \pm 4) \times 10^{-5}$	

Table 4 : Sources of prompt multilepton final states. These basically come from simultaneous pair decays or from cascade decays of botton states. Most estimates for branching ratios come from squares of branching ratios listed in Table I. Branching ratios for electron and muon final states are expected to be the same.

	Final State	Source	Branching Ratio
Opposite sign dimuons	$\mu^+\mu^-\nu\bar{\nu}$	a. double charm decay e.g. $D\bar{D}$	$(\sim 8\%)^2$
		b. double $B\bar{B}$ decay	$(\sim 10\%)^2$
	$\mu^+\mu^-\nu\bar{\nu}\nu_\tau\bar{\nu}_\tau$	c. double $\tau^+\tau^-$ decay	$(17.5\%)^2$
Same sign dimuons	$\mu^+\mu^+\nu\,\nu$ or $\mu^-\mu^-\nu\nu$	a. double decay bottom cascade e.g. $\begin{cases} B \to XD \to X\mu\nu \\ \bar{B} \to X\mu\nu \end{cases}$	$2\times(10\%)\times(8\%)$
Trimuons	$(\psi \to \mu^+\mu^-)\mu\nu$	a. double bottom decay $\begin{cases} B \to \psi \to \mu\nu \\ \bar{B} \to \mu X \text{ or } \bar{B} \to XD \to \mu \end{cases}$	$2\times 3\%\times 7\%\times(10\%+8\%)$
		b. $\psi DD \to \psi$ + extra μ	$2\times 7\%\times 8\%$
	$\mu^+\mu^-\mu^\pm\nu\nu\nu$	a. bottom cascade $B \to \mu D\nu$ $\bar{B} \to \mu\bar{D}X,\ \bar{D} \to \mu\nu X$	$2\times 10\%\times 10\%\times 8\%$
4-muons	$\mu^+\mu^-\mu^+\mu^-\nu\nu\nu\nu$	a. bottom cascade $B \to \mu DX,\ D \to \mu\nu X$ $\bar{B} \to \mu\bar{D}X,\ \bar{D} \to \mu\nu X$	$(10\%)^2\times(8\%)^2$
	$(\psi \to \mu^+\mu^-)(\psi \to \mu^+\mu^-)$	$B \to X\psi \to \mu\mu$ $\bar{B} \to \bar{X}\psi \to \mu\mu$	$(3\%)^2\times(7\%)^2$

Table 5: Acceptance calculations (ε) for different charm production models and the extracted charm cross section using the 1μ and 2μ plus missing energy data. The correlated $D\bar{D}$ production models (1a-1f) fit the data with model 1a yielding the best fit. The uncorrelated production models (2a,2b) give poor fits to the data.

					1μ data		2μ data	
Model	α	β	γ	K/K^*	ε(%)	σ(μb)	ε(%)	σ(μb)
1a	1.3	6	20	1.5	4.6	21.0	.23	14.1
1b	1.3	2	20	1.5	4.6	20.9	.40	7.9
1c	2.7	6	20	1.5	3.1	31.1	.17	19.4
1d	1.3	6	30	1.5	4.1	23.9	.20	16.0
1e	2.2	3	15	1.5	4.1	23.8	.33	9.7
1f	2.2	3	15	.67	3.5	28.0	.26	12.2
2a	2.5	3	---	1.5	2.8	35.2	.19	16.9
2b	2.5	5	---	1.5	2.4	40.8	.12	27.4

Table 6: Calculated accpetance and sensitivity for $B\bar{B}$ decay final states.

	Final State	Trigger Acceptance	Acceptance After Cuts	BR.$\sigma_{B\bar{B}}$ Per Event	BR	$\sigma_{B\bar{B}}$ Per EVENT
1a.	$\nu\mu$	65%	16%	8 pb	7.6×10^{-4}	10.7 nb
b.	$\nu\mu(P_t^\mu > 1.4)$	65%	5.6%	23 pb	7.6×10^{-4}	30.3 nb
2a.	3μ	43%	6.0%	22 pb	2.9×10^{-3}	7.6 nb
b.	3μ, $E_\nu > 30$ GeV	43%	2.7%	48 pb	2.9×10^{-3}	16.6 nb
3a.	$\mu^+\mu^+$, $E_\nu > 30$ GeV	37%	8.5%	15 pb	8.0×10^{-3}	1.9 nb
b.	$\mu^+\mu^+$, $E_\nu > 30$ GeV	37%	4.0%	33 pb	8.0×10^{-3}	4.1 nb

Table 7: Measured events and cross section limits for each $B\bar{B}$ decay final state.

	Final State	Number of Events	Background	Events	BR $\sigma_{B\bar{B}}$ (pb)	$\sigma_{B\bar{B}}$ (nb)	$\sigma_{B\bar{B}}$ 90% C.L. (n.b)
1a.	$\nu\mu$	2	3.0 ± 0.5	$-1.0^{+2.7}_{-1.4}$	-8^{+22}_{-12}	-11^{+29}_{-15}	< 26
b.	$\nu\mu$ with $p_t^{\mu} > 1.4$ GeV/c	1	$.06 \pm .04$	$.9^{+2.3}_{-.9}$	22^{+53}_{-20}	28^{+70}_{-26}	<116
2a.	3μ	19	17 ± 3	$2.0^{+6.2}_{-5.3}$	44^{+136}_{-117}	15^{+47}_{-40}	< 76
b.	3μ with $E_\nu > 30$ GeV	1	$.7 \pm .4$	$.3^{+2.4}_{-1.0}$	14^{+115}_{-48}	5^{+40}_{-17}	< 53
3a.	$\mu^+\mu^+$	92	70^{+17}_{-17}	22 ± 20	330 ± 300	41 ± 38	< 90
b.	$\mu^+\mu^+$ with $E_\nu > 30$ GeV	8	6 ± 2	$2.0^{+4.5}_{-3.4}$	66^{+149}_{-112}	8^{+19}_{-14}	< 31

Table 8 Non-prompt sources of muons (from ref. 26 and ref. 58)

Particle	(Mass MeV)	$C\tau$(cm)	Decay mode	BR
π	(139.6)	780.4	$\mu\ \nu$	100%
			$\mu\ \nu\ \gamma$	$(1.24 \pm 0.25) \times 10^{-4}$
K^+	(493.7)	370.9	$\mu\ \nu$	$(63.5 \pm 0.16)\%$
			$\mu\ \nu\ \pi^o$	$(3.2 \pm 0.09)\%$
			$\mu\ \nu\ \gamma$	$(5.8 \pm 3.5) \times 10^{-4}$
K_L^o	(497.7)	1554	$\pi\ \mu\ \nu$	$(26.8 \pm 0.5)\%$
Λ	(1115)	7.89	$p\ \mu\ \nu$	$(1.57 \pm 0.35) \times 10^{-4}$
Σ^-	(1197)	4.45	$n\ \mu^-\nu$	$(0.45 \pm 0.04) \times 10^{-3}$
Ξ^o	(1314)	8.69	$\Sigma^+\mu\ \nu$	$<3.3 \times 10^{-3}$ (Exp)
				$<3.3 \times 10^{-4}$ (RE)
Ξ^-	(1321)	4.96	$\Lambda\ \mu\ \nu$	$(3.5 \pm 3.5) \times 10^{-4}$
Ω^-	(1672)	2.47	$\Xi^o\mu^-\nu$	(0.5×10^{-2}) (TH)
			$\Xi^{o*}\mu^-\nu$	3.6×10^{-6} (TH)

Table 9 Non linearity terms in density extrapolations from finite lifetime of particles (assuming a 20 cm interaction length Λ_i) for $\Lambda d \equiv c\tau\gamma$.

Particle	Energy	γ	Λd(cm)	$\Lambda_i/\Lambda d$
π	12 GeV	86	6.7×10^4	3×10^{-4}
K	12 GeV	24	0.9×10^4	2×10^{-3}
K_L^o	20 GeV	40	6.2×10^4	3×10^{-4}
Λ	69 GeV	62	490	4×10^{-2}
Σ^-	61 GeV	51	227	9×10^{-2}
Ξ^o	94 GeV	71	617	3×10^{-2}
Ξ^-	76 GeV	58	288	7×10^{-2}
Ω^-	71 GeV	42	104	0.20

Table 10 Non-prompt sources of single electron and electron neutrinos (from Ref. 26 and Ref. 58)

Particle	$c\tau$ (cm)	Decay mode	BR
μ	6.59×10^{4}	$e\,\bar{\nu}\nu$	98.6%
		$e\,\bar{\nu}\nu\gamma$	1.4%
π	780.4	$e\nu$	$(1.267 \pm 0.023) \times 10^{-4}$
K	370.9	$e\nu\pi_o$	(4.82 ± 0.05)%
K_{oL}	1554	$\pi e\nu$	38.8%
		$\pi e\nu\gamma$	1.3%
N	2.75×10^{13}	$pe^-\nu$	100%
Λ	7.89	$pe^-\nu$	$(8.07 \pm 0.28) \times 10^{-4}$
Σ^+	2.40	$\Lambda e^+\nu$	$(2.02 \pm 0.47) \times 10^{-5}$
Σ^-	4.45	$ne^-\nu$	$(1.08 \pm 0.04) \times 10^{-3}$
		$\Lambda e^-\nu$	$(0.60 \pm 0.06) \times 10^{-4}$
Ξ^o	8.69	$\Sigma^+e^-\nu$	$<1.1 \times 10^{-3}$
Ξ^-	4.96	$\Lambda e^-\nu$	$(0.69 \pm 0.18) \times 10^{-3}$
		$\Sigma^o e^-\nu$	(0.8×10^{-4}) (TH)
Ω^-	2.47	$\Xi^o e^-\nu$	0.7×10^{-2} (TH)
		$\Xi^{o*}e^-\nu$	(0.8×10^{-5}) (TH)
		(Xev)	$\sim 10^{-2}$ (EXP)